Stem Cell Reports
Article
ISSCR
OPEN ACCESS

Ablating Adult Neural Stem Cells Improves Synaptic and Cognitive Functions in Alzheimer Models

Xiaoqin Zhang,[1,2,6] Yufei Mei,[1,3,6] Yang He,[1,3,6] Dongpi Wang,[4] Jing Wang,[1,3] Xiaojie Wei,[1,3] Enlu Yang,[1,3] Dongming Zhou,[4] Haowei Shen,[2] Guoping Peng,[1] Qiang Shu,[4] Xuekun Li,[4,5] Benyan Luo,[1] Yudong Zhou,[1,3,*] and Binggui Sun[1,3,*]

[1]Department of Neurobiology and Department of Neurology of the First Affiliated Hospital, Zhejiang University School of Medicine, Hangzhou, Zhejiang Province, 310058, China
[2]Department of Physiology and Pharmacology, Medical School of Ningbo University, Ningbo, Zhejiang Province, 315211, China
[3]NHC and CAMS Key Laboratory of Medical Neurobiology, School of Brain Science and Brain Medicine, Zhejiang University, Hangzhou, Zhejiang Province, 310058, China
[4]Children's Hospital, Zhejiang University School of Medicine, Hangzhou, Zhejiang Province, 310052, China
[5]Institute of Translational Medicine, Zhejiang University School of Medicine, Hangzhou, Zhejiang Province, 310029, China
[6]These authors contributed equally
*Correspondence: yudongzhou@zju.edu.cn (Y.Z.), bsun@zju.edu.cn (B.S.)
https://doi.org/10.1016/j.stemcr.2020.12.003

SUMMARY

Adult neurogenesis is impaired in the hippocampus of patients with Alzheimer disease (AD) as well as AD models. However, it is far from clear how modulating adult neurogenesis affects AD neuropathology. We confirm that adult hippocampal neurogenesis is impaired in two AD models. Surprisingly, however, cognitive functions are improved in AD models after ablating adult neural stem cells (aNSCs). Ablation of aNSCs does not affect the levels of amyloid β but restores the normal synaptic transmission in the dentate gyrus (DG) granule cells of AD models. Furthermore, calbindin depletion in the DG of AD mice is ameliorated after aNSC ablation, and knocking down calbindin abolishes the effects of aNSC ablation on synaptic and cognitive functions of AD mice. Together, our data suggest that cognitive functions of AD mice are improved after aNSC ablation, which is associated with the restoration of synaptic transmission in the DG granule cells with calbindin as an important mediator.

INTRODUCTION

New neurons are generated in the hippocampus of adult mammals (Boldrini et al., 2018; Eriksson et al., 1998; Kempermann et al., 2018; Kuhn et al., 2018; Lucassen et al., 2020; Moreno-Jimenez et al., 2019; Spalding et al., 2013; Tobin et al., 2019). The newly generated neurons are integrated into the pre-existing neural circuits (Anacker and Hen, 2017; van Praag et al., 2002; Vivar et al., 2012). Interestingly, in comparison with mature hippocampal granule cells (GCs), new neurons at certain developmental stages exhibit enhanced synaptic plasticity (Ge et al., 2007; Schmidt-Hieber et al., 2004), which makes them unique in modulating the activity of local neural circuits. Previous studies also indicate that new neurons are associated with a variety of cognitive functions such as learning and memory, pattern separation, mood regulation, stress, and forgetting (Akers et al., 2014; Anacker et al., 2018; Anacker and Hen, 2017; Bond et al., 2015; Clelland et al., 2009; Gu et al., 2012; Toda et al., 2019).

AD is the most common neurodegenerative disorder, characterized by extracellular deposition of amyloid β (Aβ), intracellular neurofibrillary tangles consisting of hyperphosphorylated tau, loss of neurons, synaptic deficits, and cognitive dysfunctions (Musiek and Holtzman, 2015; Selkoe and Hardy, 2016). However, the mechanisms underlying synaptic and cognitive deficits in AD are still elusive. Several studies indicate that adult neurogenesis is compromised in AD mouse models (Jin et al., 2004; Krezymon et al., 2013; Pan et al., 2016; Richetin et al., 2015; Sun et al., 2009; Unger et al., 2016) and patients with AD (Moreno-Jimenez et al., 2019; Tobin et al., 2019). Interestingly, drugs restoring adult neurogenesis in AD mice were shown to improve cognitive functions (Fiorentini et al., 2010; Wang et al., 2010). These data suggest that aberrant adult neurogenesis may account for, at least partially, the cognitive dysfunctions in AD mice. Therefore, manipulating adult neurogenesis could be a potential strategy to modulate AD pathogenesis.

A recent study demonstrated that enhancing adult neurogenesis in the presence of a healthier local brain environment but not simply increasing the number of newborn neurons ameliorated the pathology and cognitive deficits in AD mice (Choi et al., 2018), suggesting that healthy new neurons are needed to improve cognitive functions in AD. Supporting this assumption, Richetin et al. (2015) found that selective delivery of *NeuroD1* into neural progenitor cells restored dendritic spines in newborn neurons and rescued memory in AD mice. Therefore, restoring or enhancing healthy adult neurogenesis could be beneficial for AD.

The morphology (length of total or primary dendrites, dendritic complexity, spine density) and functional integration of newborn neurons were abnormal in AD mice

(Krezymon et al., 2013; Richetin et al., 2015; Sun et al., 2009). The morphologically and functionally abnormal new neurons could result in abnormal connections and aberrant activity of neural circuits in the hippocampus. Consequently, hippocampus-dependent functions would be compromised as observed in AD. We therefore hypothesized that inhibiting abnormal adult neurogenesis could be beneficial for AD as well.

To test our hypothesis, we deleted aNSCs in two AD models (APP/PS1 and hAPP-J20 mice) by a genetic approach (glial fibrillary acidic protein-thymidine kinase [GFAP-TK] mice plus treatment with ganciclovir [GCV]) or a drug-induced ablation (intraperitoneal injection of methylazoxymethanol acetate [MAM]). We then performed behavioral tests and electrophysiological recordings to evaluate the effects of aNSC ablation on cognitive functions and synaptic transmission in AD mice. In contrast to the results of two recent reports indicating that ablating adult neurogenesis exacerbated cognitive functions in AD models (Choi et al., 2018; Hollands et al., 2017), our data revealed that aNSC ablation ameliorated the cognitive and synaptic deficits in AD mice. We also identified calbindin as an important mediator during these processes.

RESULTS

Adult Hippocampal Neurogenesis Was Impaired in hAPP-J20 and APP/PS1 Mice

We demonstrated previously that the dendritic length, spine density, and functional integration of newborn neurons were abnormal in the hippocampus of hAPP-J20 versus wild type (WT) mice (Sun et al., 2009). Here we found that the number of DCX^+ cells was significantly reduced in the hippocampus of APP/PS1 versus WT mice at the ages of both 2 and 5 months (Figures 1A–1D). Although the number of hippocampal DCX^+ cells was not significantly reduced in 2- and 4-month-old hAPP-J20 mice (Figures 1E–1H), much fewer hippocampal DCX^+ cells were observed in 9-month-old hAPP-J20 versus WT mice (Figures 1I and 1J). By crossing hAPP-J20 with POMC-GFP mice (Overstreet et al., 2004), a mouse line in which newborn neurons are specifically labeled with GFP, we found less new neurons in the hippocampus of 4-month-old hAPP-J20/POMC-GFP versus WT/POMC-GFP mice (Figures 1K and 1L). Together, our results further demonstrated that adult hippocampal neurogenesis was impaired in both hAPP-J20 and APP/PS1 mice.

Genetic Approach to Inhibit Adult Neurogenesis in APP/PS1 Mice

We bred APP/PS1 with GFAP-TK mice (Snyder et al., 2011) and the offspring were treated with GCV for 4 weeks starting at the age of 2.5 months. Hippocampal DCX^+ cells were much less in TK^+ mice 7 days or 2 months after the completion of GCV treatment (Figures 2A–2D). At the age of 9 months (5 months after the completion of GCV treatment and the time of behavioral testing), no significant difference in DCX^+ cells was observed between WT/TK^- and WT/TK^+ mice. However, fewer DCX^+ cells were found in the dentate gyrus (DG) of $APP/PS1\text{-}TK^+$ versus $APP/PS1\text{-}TK^-$ mice (Figure 2E), although the reduction did not reach a statistically significant difference. While no statistically significant difference in the number of $GFAP^+/SOX2^+$ cells was observed in the SGZ (subgranular zone) between TK^- and TK^+ mice after GCV treatment (Figures S1A and S1B), the number of $GFAP^+/Ki67^+$ cells was dramatically reduced in TK^+ mice versus TK^- mice (Figures S1C and S1D), suggesting that loss of active but not silent aNSCs mainly accounts for the reduced DCX^+ neurons in GCV-treated TK^+ mice.

There was no difference in the number of either microglia ($Iba1^+$) or astrocytes ($GFAP^+$ or $ALDH1L1^+$) in the hippocampus between TK^- and TK^+ mice 7 days (Figures S2A–S2C, S2E–S2G, and S2I) or 5 months (Figures S2J–S2L and S2O–S2Q) after the completion of GCV treatment. More astrocytes and microglia were observed in the hippocampus of mice with APP/PS1 background versus WT background at around 9 months old (Figures S2L and S2Q). Sholl analysis revealed that the morphology of astrocytes and microglia was similar in the hippocampus between TK^- and TK^+ mice after GCV treatment (Figures S2D, S2H, S2M, S2N, S2R, and S2S).

Although the number of DCX^+ cells was reduced in the hippocampus of APP/PS1 (Figures 1A–1D), curiously, however, no difference in DCX^+ cells was observed between $WT\text{-}TK^-$ and $APP/PS1\text{-}TK^-$ mice (Figures 2B–2E). Crossing with GFAP-TK mice may somehow affect the DCX expression in APP/PS1 mice. The relative resistance to DCX reduction in APP/PS1 mice on a mixed C57Bl/6:CD-1 background likely reflects heterosis, or hybrid vigor, a well-documented phenomenon in plants and mammals (Comings and MacMurray, 2000). We then analyzed the morphology of newborn neurons using a retroviral vector expressing enhanced GFP (eGFP) (Zhao et al., 2006). We found that the dendrites were shorter and the spine density was lower in new neurons of $APP/PS1\text{-}TK^-$ versus $WT\text{-}TK^-$ mice (4 months old) (Figures S3A–S3D), suggesting impaired adult neurogenesis in $APP/PS1\text{-}TK^-$ mice.

Genetic Ablation of aNSCs Improved Spatial Learning and Memory in APP/PS1 Mice

As reflected by the escape latency to the hidden platform in the Morris water maze (MWM) test, WT mice learned the task quickly (Figure 2F). However, the spatial learning was considerably impaired in 8–10-month-old APP/PS1 mice

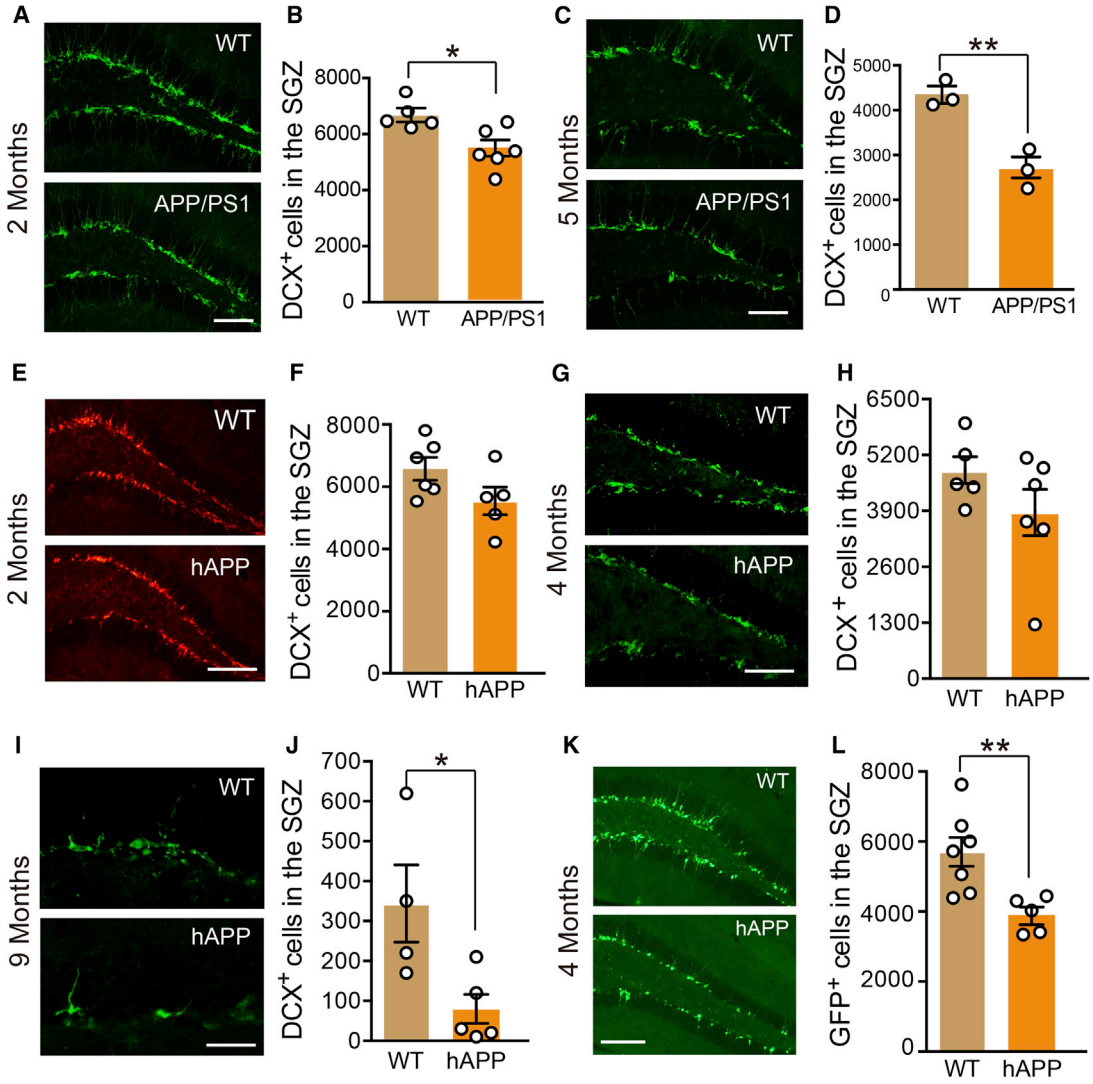

Figure 1. Adult Neurogenesis was Impaired in the Hippocampus of APP/PS1 and hAPP-J20 Mice

(A) Hippocampal DCX$^+$ cells in 2-month-old WT and APP/PS1 mice. Scale bar, 100 μm.

(B) Quantification of DCX$^+$ cells in 2-month-old WT (n = 5) and APP/PS1 (n = 6) mice. *p < 0.05 (unpaired t test), data are represented as mean ± SEM.

(C) Hippocampal DCX$^+$ cells in 5-month-old WT and APP/PS1 mice. Scale bar, 100 μm.

(D) Quantification of DCX$^+$ cells in 5-month-old WT (n = 3) and APP/PS1 (n = 3) mice. **p < 0.01 (unpaired t test), data are represented as mean ± SEM.

(E) Hippocampal DCX$^+$ cells in 2-month-old WT and hAPP-J20 mice. Scale bar, 100 μm.

(F) Quantification of DCX$^+$ cells in 2-month-old WT (n = 6) and hAPP-J20 (n = 5) mice. Unpaired t test, data are represented as mean ± SEM.

(G) Hippocampal DCX$^+$ cells in 4-month-old WT and hAPP-J20 mice. Scale bar, 100 μm.

(H) Quantification of DCX$^+$ cells in 4-month-old WT (n = 5) and hAPP-J20 (n = 6) mice. Unpaired t test, data are represented as mean ± SEM.

(I) Hippocampal DCX$^+$ cells in 9-month-old WT and hAPP-J20 mice. Scale bar, 100 μm.

(J) Quantification of DCX$^+$ cells in 9-month-old WT (n = 4) and hAPP-J20 (n = 5) mice. *p < 0.05 (unpaired t test), data are represented as mean ± SEM.

(K) GFP$^+$ cells in the hippocampus of 4-month-old WT/POMC-GFP and hAPP-J20/POMC-GFP mice. Scale bar, 100 μm.

(L) Quantification of GFP$^+$ cells in the DG of 4-month-old WT/POMC-GFP (n = 7) and hAPP-J20/POMC-GFP (n = 5) mice. **p < 0.01 (unpaired t test), data are represented as mean ± SEM.

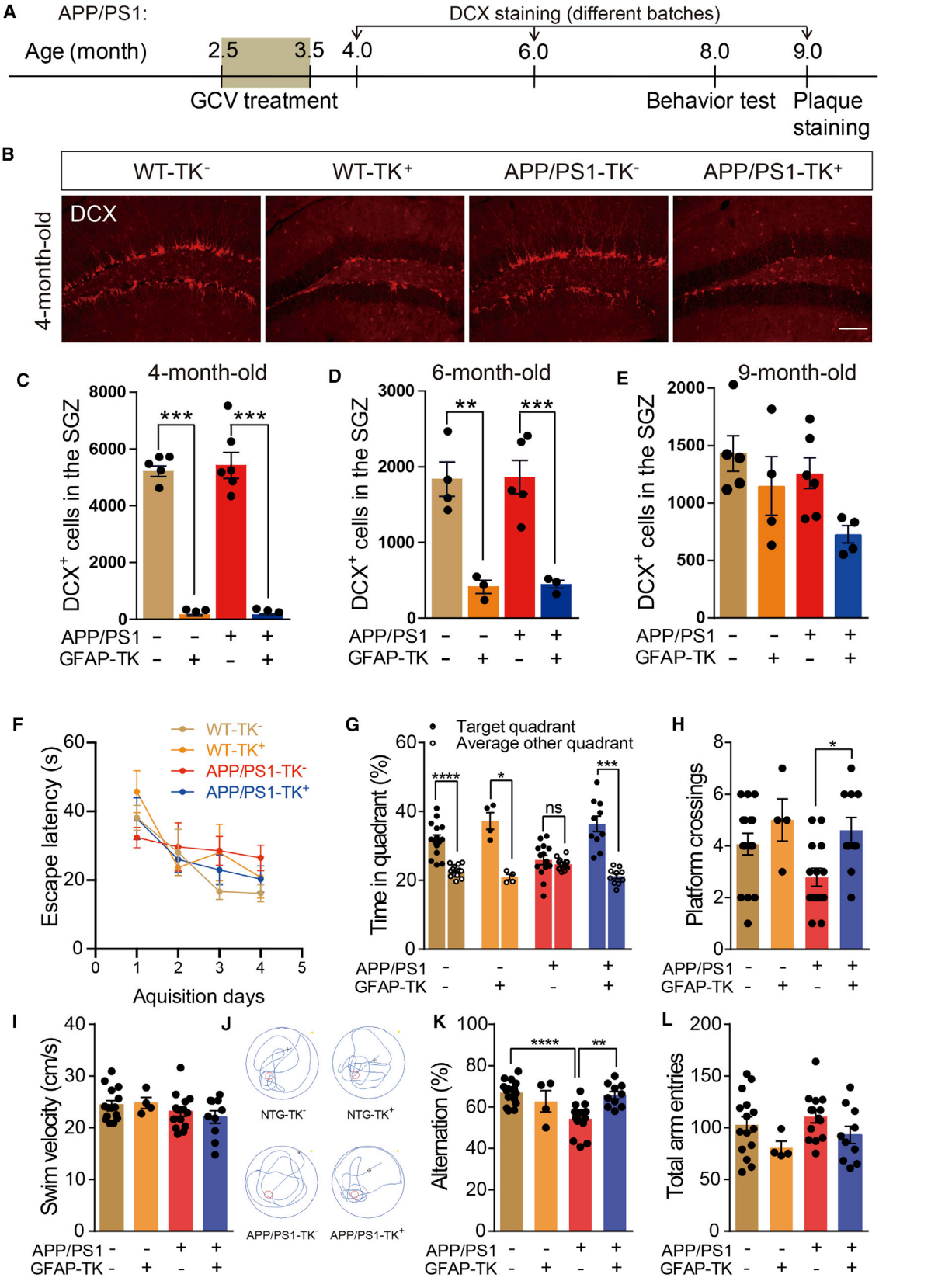

(legend on next page)

(Figure 2F). Interestingly, the escape latency was shorter for APP/PS1-TK$^+$ versus APP/PS1-TK$^-$ mice after GCV treatment (Figure 2F), suggesting that spatial learning was improved in APP/PS1 mice after aNSC ablation. The swimming speed was similar among different groups of mice (Figure 2I). As reflected by the platform crossings and the time spent in the target quadrant in probe trials, the memory retention was significantly impaired in APP/PS1 mice (Figures 2G and 2H) and it was greatly improved after aNSC ablation (Figures 2G and 2H).

In Y-maze test, the total number of individual arm entries was not altered among different groups (Figure 2L). A lower spontaneous alternation percentage was observed in APP/PS1 mice (Figure 2K), suggesting impaired short-term spatial working memory. However, the short-term spatial working memory was improved in APP/PS1 mice after aNSC ablation (Figure 2K).

Drug-Induced Ablation of aNSCs Improved Spatial Memory in AD Mice

To further examine the effects of aNSC ablation on cognitive functions in AD mice, we treated hAPP-J20 mice with MAM, a DNA methylating agent and a toxin for proliferating cells (Shors et al., 2001), as an alternative approach to ablate aNSCs. hAPP-J20 but not APP/PS1 mice were used based on the following considerations: (1) learning and memory deficits are observed in hAPP-J20 mice at 4–5 months when adult neurogenesis is still active, but cognitive deficits cannot be observed in APP/PS1 mice until 8 months, when the number of aNSCs is dramatically reduced; (2) the effect of MAM treatment on the ablation of aNSCs is not long lasting compared with GFAP-TK/GCV ablation. Therefore, early treatment with MAM may not have effects on spatial learning and memory in 8-month-old APP/PS1 mice, and late treatment with MAM would only have a minor impact on aNSCs.

MAM treatment induced effective ablation of aNSCs in the DG of both WT and hAPP-J20 mice (4.5–5 months old) (Figures 3A–3C). Although there is no difference in DCX$^+$ cells in the DG between WT/veh and hAPP-J20/veh mice (Figures 3B and 3C), both dendritic length and spine density were reduced in newborn neurons of hAPP-J20/veh versus WT/veh (Figures S3E–S3H), indicating that newborn neurons are abnormal in hAPP-J20/veh mice. MAM treatment did not affect the number and morphology of hippocampal microglia and astrocytes in both WT and hAPP-J20 mice (Figures S4A–S4I).

In the MWM test, the ability of spatial learning was significantly impaired in hAPP-J20 (Figure 3D). Although we did not find a statistically significant effect, there was a trend of recovery in terms of the spatial learning in hAPP-J20 mice after aNSC ablation (Figure 3D). Meanwhile, there is a trend of worsening spatial learning in the WT mice after ablating aNSCs (Figure 3D). In the MWM probe trial and Y-maze test, spatial memory was impaired in hAPP-J20 but was significantly improved after MAM treatment (Figures 3E, 3F, and 3H). Ablating aNSCs, however, impaired spatial memory in WT mice (Figures 3E and 3H). The swimming speed was similar among different groups of mice (Figure 3G). These data further confirmed that aNSC ablation ameliorated the cognitive deficits in AD mice.

Ablation of aNSCs Did Not Affect Aβ Pathology in AD Mice

For 9-month-old (5 months after the completion of GCV treatment) and 4–5-month-old (7 days after the completion of GCV treatment) mice, the levels of full-length and

Figure 2. Genetic Ablation of aNSCs Improved Spatial Learning and Memory in APP/PS1 Mice

(A) Timeline for the experiments.

(B) DCX$^+$ cells in the hippocampus of mice 7 days after the completion of GCV treatment. Scale bar, 100 μm.

(C–E) Quantification of DCX$^+$ cells in the DG of mice 7 days (C), 2 months (D), and 5 months (E) after the completion of GCV treatment. Two-way ANOVA with Bonferroni post tests, data are represented as mean ± SEM. **p < 0.01, ***p < 0.001.

(F–J) Effects of ablating aNSCs on learning and memory in MWM (WT-TK$^-$, n = 15; WT-TK$^+$, n = 4; APP/PS1-TK$^-$, n = 14; APP/PS1-TK$^+$, n = 10; 8–10 months of age). (F) Hidden platform learning curves. *p < 0.05 by repeated-measures ANOVA and Bonferroni post hoc test, data are represented as mean ± SEM. (G) Percentage of time spent in the target and other quadrants. *p < 0.05, ***p < 0.001, ****p < 0.0001 (target versus average of other quadrants, two-tailed paired t test). Data are represented as mean ± SEM. (H) Number of target platform crossings, a two-way ANOVA analysis identified a significant effect of ablating aNSCs on memory of APP/PS1 mice ($F_{(1,39)}$ = 6.726, p = 0.0133), *p < 0.05, Bonferroni post hoc test, data are represented as mean ± SEM. (I) Swimming speed during the pre-training test. Two-way ANOVA with Bonferroni post hoc test, data are represented as mean ± SEM. (J) Swimming traces during the probe test.

(K and L) Effects of ablating aNSCs on memory in Y-maze test (WT-TK$^-$, n = 15; WT-TK$^+$, n = 4; APP/PS1-TK$^-$, n = 14; APP/PS1-TK$^+$, n = 10; 8–10 months old).

(K) Percentage of alternation on Y-maze test. Two-way ANOVA: genotype (APP or WT), $F_{(1,39)}$ = 4.042, p = 0.0513; ablating aNSCs, $F_{(1,39)}$ = 2.221, p = 0.1442; interaction, $F_{(1,39)}$ = 10.46, p = 0.0025; **p < 0.01, ****p < 0.0001 with Bonferroni post hoc test. Data are represented as mean ± SEM.

(L) Total entry numbers into each arm of Y-maze test. Two-way ANOVA with Bonferroni post hoc test, data are represented as mean ± SEM. See also Figures S1–S3.

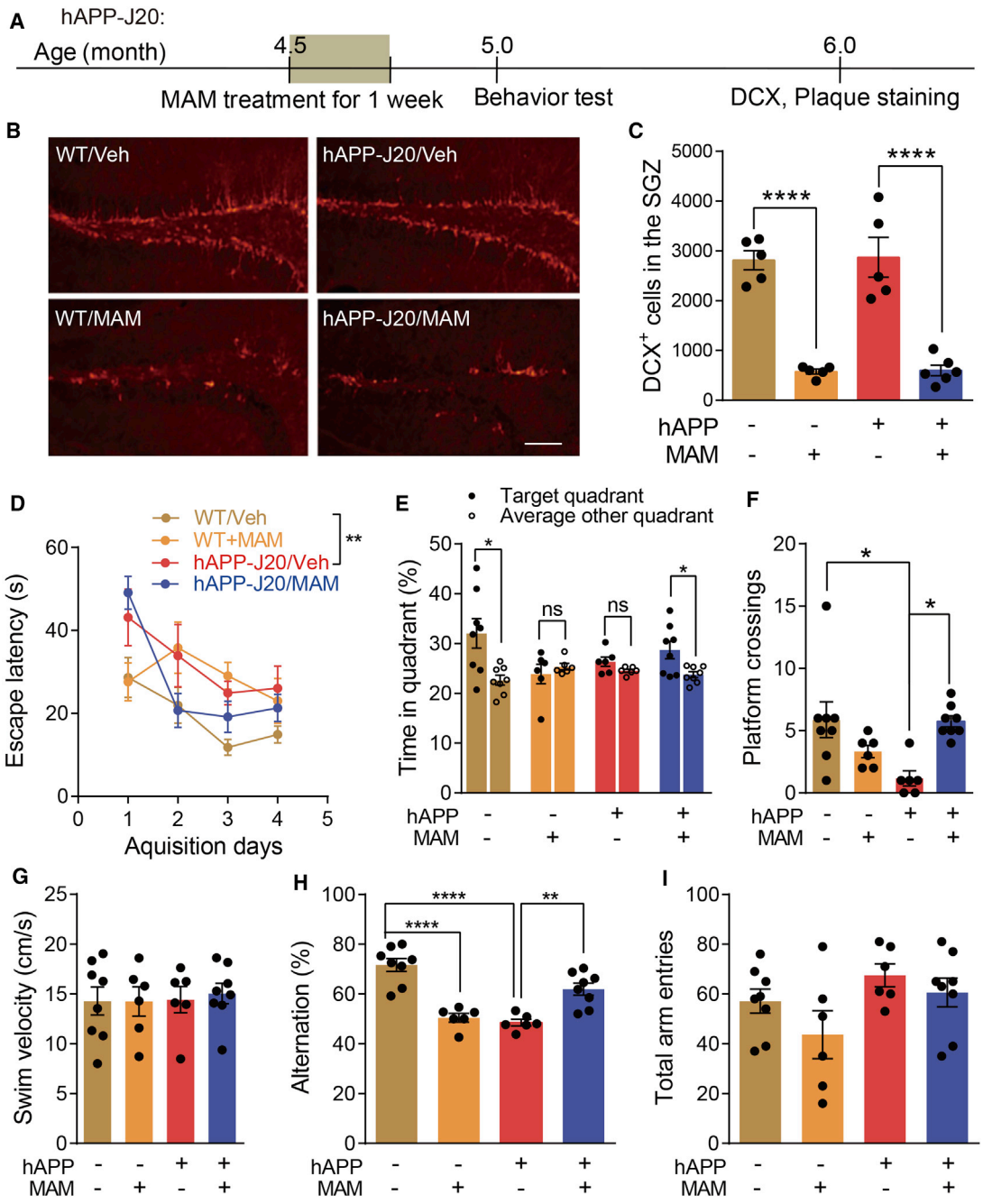

Figure 3. Ablating aNSCs by MAM Treatment Improved Spatial Learning and Memory in hAPP-J20 Mice

(A) Timeline for the experiments.

(B) DCX$^+$ cells in the hippocampus of mice before and after MAM treatment. Scale bar, 100 μm.

(C) Quantification of DCX$^+$ cells in the DG of WT/veh (n = 5), WT/MAM (n = 5), hAPP/veh (n = 5), and hAPP/MAM (n = 6) mice. Two-way ANOVA with Bonferroni post tests, data are represented as mean ± SEM. ****p < 0.0001.

(D–G) Effects of ablating aNSCs on learning and memory in MWM test (WT/veh, n = 8; WT/MAM, n = 6; hAPP-J20/veh, n = 6; hAPP-J20/MAM, n = 8; 5–6 months of age). (D) Hidden platform learning curves. **p < 0.01 by repeated-measures ANOVA and Bonferroni post hoc test, data are represented as mean ± SEM. (E) Percentage of time spent in the target and other quadrants, *p < 0.05 (target versus average of other quadrants, two-tailed paired t test). Data are represented as mean ± SEM. (F) Number of target platform crossings, two-way ANOVA: genotype × treatment, $F_{(1,24)} = 14.25$, p = 0.0009; genotype, $F_{(1,24)} = 1.474$, p = 0.2365; treatment, $F_{(1,24)} = 1.170$, p = 0.2901; *p < 0.05

(legend continued on next page)

C-terminal fragments (α- or β-CTF) of hAPP and Aβ levels were similar between APP/PS1-TK$^-$ and APP/PS1-TK$^+$ mice (Figures 4C–4H). Aβ plaque load was similar in the hippocampus of 9-month-old APP/PS1 mice with or without aNSC ablation (Figures 4A and 4B). We did not compare the Aβ plaques of 4–5-month-old mice because they are absent in the hippocampus of APP/PS1 mice at this stage (Minkeviciene et al., 2008).

APP/PS1 mice carry transgenes of human APP and human presenilin-1 (PS1) with AD-linked mutations (Jankowsky et al., 2004). We therefore examined the expression of PS1 after aNSC ablation. The expression of PS1 in the hippocampus was similar between APP/PS1-TK$^-$ and APP/PS1-TK$^+$ mice 7 days after the completion of GCV treatment (Figures S5A and S5B). However, higher levels of PS1 were observed in APP/PS1-TK$^+$ mice versus APP/PS1-TK$^-$ mice 5 months after the completion of GCV treatment (Figures S5C and S5D).

Similarly, MAM-induced ablation of aNSCs did not affect the Aβ plaques, full-length and CTFs of hAPP, and Aβ levels in the hippocampus of hAPP-J20 mice (around 6 months old) (Figures 4I–4M). Genetic ablation of aNSCs did not affect the levels of full-length and CTFs of hAPP and Aβ levels, either (Figures 4N–4P). We did not compare the Aβ deposition between hAPP-J20/TK$^-$ and hAPP-J20/TK$^+$ mice after GCV treatment because Aβ plaques were barely observed in the brain of hAPP-J20 mice younger than 5.5 months (Mucke et al., 2000).

Taken together, these data indicated that ablation of aNSCs did not affect the Aβ deposition, hAPP processing, or Aβ levels in the hippocampus of AD mice.

Restoration of Normal Synaptic Transmission in the DG of AD Mice after aNSC Ablation

Similar to previous reports showing increased inhibition in hippocampal GCs of AD mice (Palop et al., 2007), we found that the amplitudes of evoked and miniature excitatory postsynaptic currents (eEPSCs and mEPSCs) were smaller (Figures 5A, 5C, and 5E) and the amplitudes of evoked and miniature inhibitory postsynaptic currents (eIPSCs and mIPSCs) were larger (Figures 5B, 5D, and 5F) in the GCs of hAPP-J20 mice versus WT mice (5–6 months), suggesting increased response to inhibitory synaptic transmission but decreased response to excitatory synaptic transmission in the GCs of hAPP-J20 mice. The amplitudes of both mIPSC and eIPSC in the GCs of hAPP-J20 mice were decreased to similar levels to those of WT mice after aNSC ablation (Figures 5B, 5D, and 5F). Meanwhile, the amplitudes of both mEPSC and eEPSC in the GCs of hAPP-J20 mice were increased to normal levels after aNSC ablation (Figures 5A, 5C, and 5E), suggesting that aNSCs may contribute to the abnormal synaptic transmission in hAPP-J20 mice.

To further examine the effect of aNSC ablation on the synaptic transmission in the DG of AD mice, we again turned to another AD model (APP/PS1). Similar to hAPP-J20 mice, the amplitude of eEPSC was significantly decreased while the amplitude of eIPSC was significantly increased in the GCs of APP/PS1 versus WT mice (around 4 months old), and aNSC ablation corrected these changes (Figures 6A and 6B). Ablating aNSCs also reversed the changes of mEPSC and mIPSC in APP/PS1 mice (Figures 6C–6H). These results indicated that the abnormal adult neurogenesis might contribute to abnormal synaptic transmission in the DG of APP/PS1 mice, as well.

As additional evidence to support this conclusion, we found that aNSC ablation significantly reduced the frequency of spontaneous inhibitory postsynaptic currents (sIPSCs) and diminished the action-potential (AP)-driven IPSC frequency (subtracting mIPSC from sIPSC) in the GCs of hAPP-J20 mice (Figure S6).

Taken together, these data demonstrated that aNSC ablation prevented the abnormal synaptic transmission in the DG of AD mice.

Calbindin Deletion in the DG of AD Mice Was Attenuated after Ablating aNSCs

The expression of calbindin-D28k, a calcium-binding protein, was significantly decreased in the DG of both AD patients and AD models (Palop et al., 2003; Sun et al., 2008), and the calbindin depletion was associated with synaptic and cognitive deficits in AD mice (Palop et al., 2003; Sanchez et al., 2012; You et al., 2017). We therefore wondered whether alterations in calbindin expression were involved in the beneficial effects of aNSC ablation in AD mice. Consistent with previous reports (Palop et al., 2003; Sun et al., 2008), we found that the expression of calbindin was significantly reduced in the DG of APP/PS1 (Figures S7A and S7B) and hAPP-J20 mice (Figures 7A and 7B) versus

with Bonferroni post hoc test. Data are represented as mean ± SEM. (G) Swimming speed during the pre-training test. Two-way ANOVA with Bonferroni post hoc test, data are represented as mean ± SEM.

(I and J) Effects of ablating aNSCs on memory in Y-maze test (WT/veh, n = 8; WT/MAM, n = 6; hAPP-J20/veh, n = 6; hAPP-J20/MAM, n = 8; 5–6 months of age). (I) Percentage of alternation in Y-maze test, two-way ANOVA: genotype × treatment, $F_{(1,24)} = 57.52$, $p < 0.0001$; genotype, $F_{(1,24)} = 6.460$, $p = 0.0179$; treatment, $F_{(1,24)} = 2.899$, $p = 0.1016$; $^{**}p < 0.01$, $^{****}p < 0.0001$ with Bonferroni post hoc test. Data are represented as mean ± SEM. (J) Total entry numbers into each arm of Y-maze test. Two-way ANOVA with Bonferroni post hoc test, data are represented as mean ± SEM.

See also Figures S3 and S4.

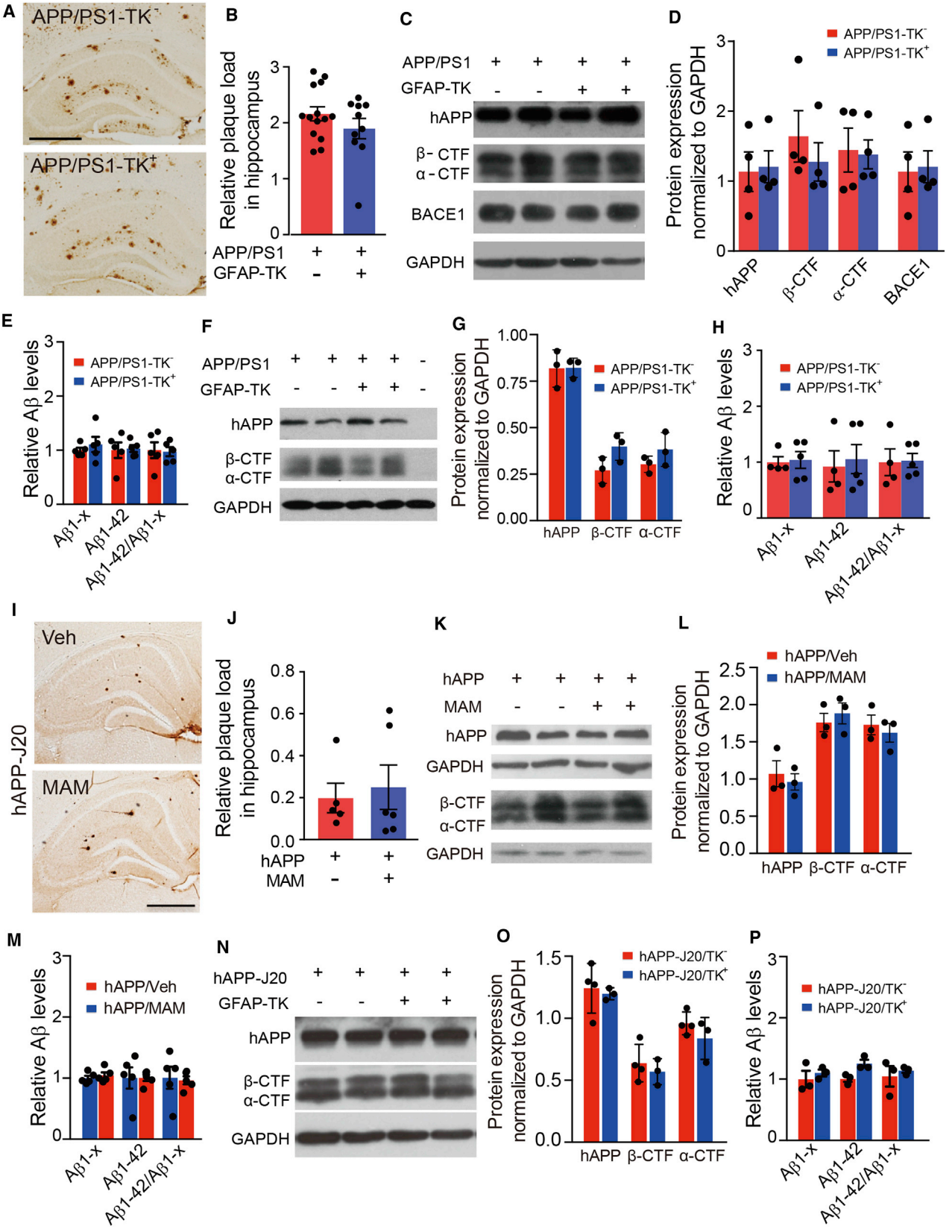

(legend on next page)

WT mice. However, this reduction was greatly attenuated after genetic ablation of aNSCs (Figures 7A, 7B, S7A, and S7B), suggesting that altered expression of calbindin was associated with the effects of aNSC ablation on synaptic and cognitive functions in AD models.

To further explore why the expression of calbindin was recovered in the DG of AD mice after aNSC ablation, we examined the expression of ΔFosB, a highly stable transcription factor, and its elevated expression was associated with seizure activity and contributed to the suppression of calbindin in the DG of hAPP-J20 mice (You et al., 2017). Consistent with this study (You et al., 2017), we found that the expression of ΔFosB was significantly increased in the DG of hAPP-J20 mice (Figures S7C and S7D). Interestingly, the elevated expression of ΔFosB was attenuated after aNSC ablation (Figures S7C and S7D), suggesting that reduced ΔFosB may contribute to the recovery of calbindin in the DG of hAPP-J20 mice after aNSC ablation.

Hippocampal Knockdown of Calbindin Abolished the Effects of aNSC Ablation on Synaptic and Cognitive Functions in hAPP-J20 Mice

To directly test the possibility that the altered expression of calbindin was associated with the effects of aNSC ablation on synaptic and cognitive functions in AD models, we injected AAV-shCalb1 (Li et al., 2017) into the DG of hAPP-J20 mice after genetically ablating aNSCs to knock down the expression of calbindin. As shown in Figures 7A and 7B, AAV-shCalb1 but not AAV-control virus successfully reduced the expression of calbindin in the DG of aNSCs-deleted hAPP-J20 mice. Genetic ablation of aNSCs did not affect the number and morphology of microglia and astrocytes in the hippocampus of hAPP-J20 mice (Figures S4J–S4R).

Whole-cell recordings in the presence of tetrodotoxin revealed that the amplitudes of mIPSC and mEPSC in GCs of hAPP-J20 mice (5–6 months old) were increased and decreased, respectively, when compared with WT mice, and aNSC ablation prevented these changes (Figures 7C–7H). Interestingly, reducing the expression of calbindin by AAV-shCalb1 abolished the effects of aNSC ablation on mIPSC and mEPSC in GCs of hAPP-J20 mice (Figures 7C–7H).

Next, we tested the memory of mice in the Y maze. Spatial memory was impaired in hAPP-J20 mice and it was improved after genetic ablation of aNSCs (Figures 7I and 7J). This is consistent with the results in APP/PS1 mice (Figure 2) and in drug-treated hAPP-J20 mice (Figure 3). However, knockdown of calbindin abolished the beneficial effects of aNSC ablation (Figures 7I and 7J).

Figure 4. Ablating aNSCs Did Not Affect the Aβ Pathology

(A) 3D6-positive plaques in the hippocampus of 9-month-old APP/PS1-TK$^-$ and APP/PS1-TK$^+$ mice treated with GCV. Scale bar, 100 μm.
(B) Quantification of the plaque load in the hippocampus of 9-month-old APP/PS1-TK$^-$ (n = 14) and APP/PS1-TK$^+$ mice (n = 10) treated with GCV. Unpaired t test, data are represented as mean ± SEM.
(C) Western blot analysis of hAPP (6E10), β-CTF and α-CTF (CT-15), and BACE1 in the hippocampus of 9-month-old APP/PS1-TK$^-$ and APP/PS1-TK$^+$ mice treated with GCV. GAPDH served as the loading control.
(D) Quantification of the bands shown in (C), n = 4 mice for each group. Unpaired t test, data are represented as mean ± SEM.
(E) Comparison of human Aβ1-42 and Aβ1-x levels by ELISA in the hippocampus of 9-month-old APP/PS1-TK$^-$ and APP/PS1-TK$^+$ mice treated with GCV. n = 5 mice for each group. Unpaired t test, data are represented as mean ± SEM.
(F) Western blot analysis of hAPP, β-, and α-CTFs in the hippocampus of 5-month-old APP/PS1-TK$^-$ and APP/PS1-TK$^+$ mice treated with GCV. GAPDH served as the loading control.
(G) Quantification of the bands shown in (F), n = 3 mice for each group. Unpaired t test, data are represented as mean ± SEM.
(H) Comparison of human Aβ1-42 and Aβ1-x levels in the hippocampus of 5-month-old APP/PS1-TK$^-$ (n = 4) and APP/PS1-TK$^+$ mice (n = 5) treated with GCV. Unpaired t test, data are represented as mean ± SEM.
(I) 3D6-positive plaques in the hippocampus of 6-month-old hAPP-J20 mice treated with veh or MAM. Scale bar, 500 μm.
(J) Quantification of the plaque load in the hippocampus of hAPP-J20 mice. hAPP-J20/veh, n = 5; hAPP-J20/MAM, n = 6. Unpaired t test, data are represented as mean ± SEM.
(K) Western blot analysis of hAPP, β-, and α-CTFs in the hippocampus of 6-month-old hAPP-J20 mice treated with veh or MAM. GAPDH served as the loading control.
(L) Quantification of the bands shown in (K), n = 3 mice for each group. Unpaired t test, data are represented as mean ± SEM.
(M) Comparison of human Aβ1-42 and Aβ1-x levels in the hippocampus of 6-month-old hAPP-J20 mice treated with MAM. n = 5 mice for each group. Unpaired t test, data are represented as mean ± SEM.
(N) Western blot analysis of hAPP, β-, and α-CTFs in the hippocampus of hAPP-J20/TK$^-$ and hAPP-J20/TK$^+$ mice treated with GCV. GAPDH served as the loading control.
(O) Quantification of the bands shown in (N), n = 4 (hAPP-J20/TK$^-$) and 3 (hAPP-J20/TK$^+$). Unpaired t test, data are represented as mean ± SEM.
(P) Comparison of human Aβ1-42 and Aβ1-x levels in the hippocampus of 5-month-old hAPP-J20/TK$^-$ and hAPP-J20/TK$^+$ mice treated with GCV. n = 3 mice for each group. Unpaired t test, data are represented as mean ± SEM.
See also Figure S5.

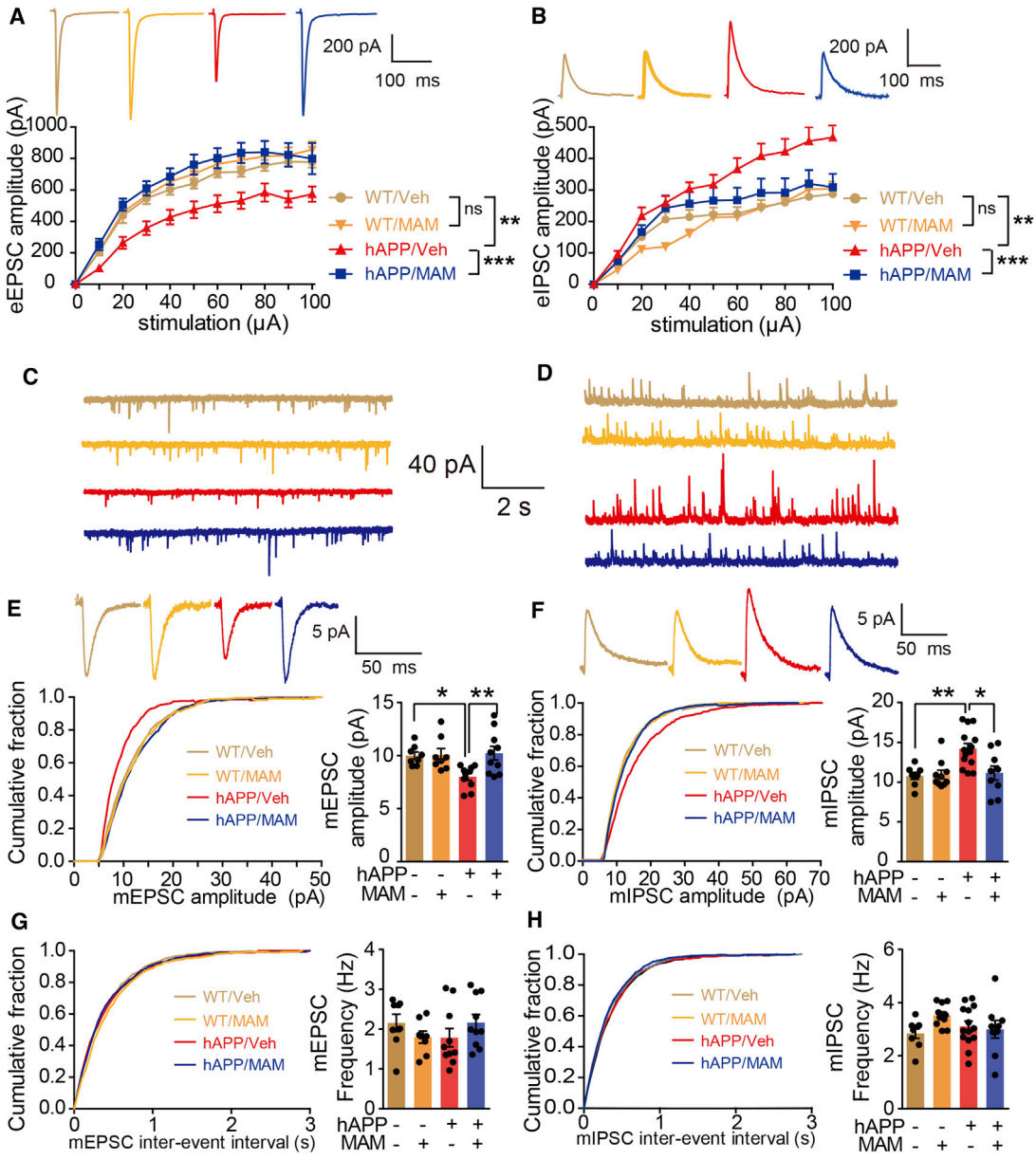

Figure 5. Ablating aNSCs by MAM Restored the Synaptic Transmission in DG GCs of hAPP-J20 Mice

(A) Traces of eEPSCs and quantification of eEPSC amplitudes in GCs. WT/veh (n = 12 cells from three mice), WT/MAM (n = 11 cells from three mice), hAPP/veh (n = 13 cells from three mice), and hAPP/MAM (n = 13 cells from three mice). **p < 0.01, ***p < 0.001, two-way ANOVA with Bonferroni post hoc test, data are represented as mean ± SEM.

(B) Traces of eIPSCs and quantification of eIPSC amplitudes in GCs. WT/veh (n = 8 cells from three mice), WT/MAM (n = 10 cells from three mice), hAPP/veh (n = 13 cells from three mice), and hAPP/MAM (n = 13 cells from three mice). **p < 0.01, ***p < 0.001, two-way ANOVA with Bonferroni post tests, data are represented as mean ± SEM.

(C and D) Traces of mEPSCs (C) and mIPSCs (D) recorded in GCs of WT/veh, WT/MAM, hAPP/veh, and hAPP/MAM mice.

(E and G) Cumulative fraction plots and quantification of mEPSC amplitude (E) and frequency (G) in GCs of WT/veh (n = 8 cells from three mice), WT/MAM (n = 8 cells from three mice), hAPP/veh (n = 10 cells from three mice), and hAPP/MAM (n = 10 cells from three mice) mice. Two-way ANOVA for (E): genotype, $F_{(1,34)}$ = 2.959, p = 0.0945; treatment, $F_{(1,34)}$ = 6.584, p = 0.0149; interaction, $F_{(1,34)}$ = 5.707, p = 0.0226; *p < 0.05, **p < 0.01 with Bonferroni post hoc test. Data are represented as mean ± SEM.

(F and H) Cumulative fraction plots and quantification of mIPSC amplitude (F) and frequency (H) in GCs of WT/veh (n = 8 cells from three mice), WT/MAM (n = 10 cells from three mice), hAPP/veh (n = 14 cells from three mice), and hAPP/MAM (n = 9 cells from three mice) mice.

(legend continued on next page)

Taken together, our results demonstrated that the altered expression of calbindin mediated the effects of aNSC ablation on synaptic and cognitive functions in hAPP-J20 mice.

DISCUSSION

We demonstrated that ablation of aNSCs by GFAP-TK/GCV or MAM treatment improved cognitive functions in two mouse models of AD. Both GFAP-TK/GCV and MAM treatment may kill the proliferating glial cells. GCV treatment alone was also reported to inhibit the activation of microglia (Ding et al., 2014; Mathur et al., 2017). It is unlikely, however, that the improved cognitive functions in AD mice in the current study were caused by reduced gliosis: (1) TK^+ mice were treated with GCV at the age of 2–4 months when proliferative astrocytes and microglia are barely observed in the hippocampus for both APP/PS1 and hAPP-J20 mice (Jackson et al., 2013; Minkeviciene et al., 2008; Wright et al., 2013); (2) both TK^- and TK^+ mice of APP/PS1 and hAPP-J20 were treated with GCV in the current study; (3) hAPP-J20 mice were treated with MAM at the age of 4.5–5 months when gliosis is minimal (Wright et al., 2013). Actually, no difference in the number and morphology of microglia and astrocytes was observed in the hippocampus between TK^- and TK^+ mice of APP/PS1 or hAPP-J20, or veh- and MAM-treated hAPP-J20 mice.

Although the expression of PS1 was increased in the hippocampus of old APP/PS1-TK^+ mice, the Aβ plaque load, processing of hAPP, and Aβ levels were not affected in the hippocampus of young or old APP/PS1-TK^+ mice after GCV treatment. They were not affected, either, in MAM-treated hAPP-J20 mice or hAPP-J20/TK^+ mice after GCV delivery. Therefore, the improved cognitive functions in AD mice were not due to reduced Aβ pathology.

We found that aNSC ablation restored normal synaptic transmission and, particularly, prevented the increased inhibition in the GCs of AD mice, suggesting that abnormal aNSCs or new neurons derived from them might drive the aberrant activity of inhibitory neurons in the hippocampus of AD mice. This is consistent with previous reports showing that adult-born new neurons activate GABAergic neurons and exert a net inhibitory effect on the local neural circuits in the hippocampus (Anacker and Hen, 2017; Drew et al., 2016). GCs are an important component of the neural circuit in the hippocampus. Therefore, restoring synaptic transmission in GCs after aNSC ablation is expected to improve the function of the hippocampal neural circuit in AD mice, which may account for the effects of aNSC ablation on cognitive functions in AD models. In future studies, the effects of ablating aNSCs on the activity of GABAergic neurons in the hippocampus of AD mice need to be assessed.

Calbindin is critical for hippocampal function and memory (Molinari et al., 1996). Decreased expression of calbindin was associated with the remodeling of hippocampal circuits and synaptic and cognitive deficits in AD models (Palop et al., 2003, 2007; Sanchez et al., 2012; You et al., 2017). Previous studies showed that elevated expression of ΔFosB induced by seizure activity contributed to the suppression of calbindin in the DG of hAPP-J20 mice (You et al., 2017), and ablation of aNSCs led to a reduction of chronic seizure frequency (Cho et al., 2015). We found that aNSC ablation prevented the elevated expression of ΔFosB in the DG of hAPP-J20 mice, suggesting that ablation of aNSCs may reduce the seizure activity in AD mice, which may lead to decreased expression of ΔFosB and then result in recovery of calbindin. While more work is needed to demonstrate whether ablation of aNSCs will reduce the seizure activity in AD mice, our finding that knocking down the expression of calbindin abolished the effects of aNSC ablation on synaptic transmission demonstrated that the recovery of calbindin induced by aNSC ablation was essential for the restoration of normal synaptic transmission in the GCs of AD mice.

Our data are seemingly in contradiction with previous studies reporting that enhancing adult neurogenesis is associated with improved cognitive functions in AD mice (Choi et al., 2018; Fiorentini et al., 2010; Richetin et al., 2015; Wang et al., 2010). However, we believe that the effects of deleting abnormal new neurons and enhancing healthy new neurons on AD pathology are not mutually exclusive: (1) enhancing adult neurogenesis plus exercise or brain-derived neurotrophic factor (BDNF) but not enhancing adult neurogenesis alone improves cognitive functions in AD mice (Choi et al., 2018). Both exercise and BDNF are known to improve the hippocampal microenvironment, which supports the generation and survival of healthy newborn neurons (Scharfman et al., 2005; van Praag et al., 1999); (2) restoring dendritic spines without increasing the overall number of new neurons after overexpression of NeuroD1 in aNSCs rescues spatial memory in AD mice (Richetin et al., 2015); (3) as shown in our current study, ablating aNSCs restores the normal synaptic transmission in the GCs of AD mice, suggesting that abnormal new neurons may contribute to the aberrant synaptic transmission that is associated with the dysfunction of hippocampal neural circuits and hippocampus-dependent

Two-way ANOVA for (F): genotype, $F_{(1,37)} = 7.078$, $p = 0.0115$; treatment, $F_{(1,37)} = 4.536$, $p = 0.0399$; interaction, $F_{(1,37)} = 5.666$, $p = 0.0226$; *$p < 0.05$, **$p < 0.01$ with Bonferroni post hoc test. Data are represented as mean ± SEM.
See also Figure S6.

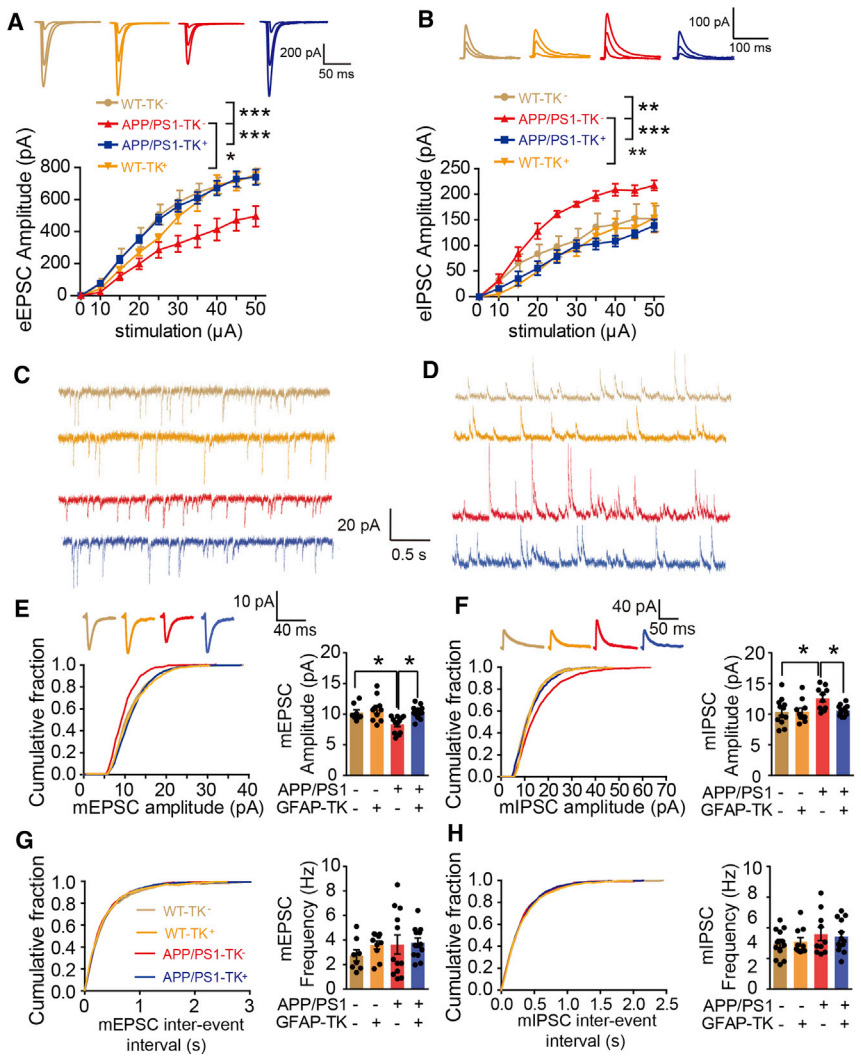

Figure 6. Genetic Ablation of aNSCs Restored the Synaptic Transmission in DG GCs of APP/PS1 Mice

(A) Traces of eEPSCs and quantification of eEPSC amplitudes recorded in GCs of mice treated with GCV (WT-TK$^-$, n = 11 cells from four mice; WT-TK$^+$, n = 8 cells from four mice; APP/PS1-TK$^-$, n = 8 cells from three mice; APP/PS1-TK$^+$, n = 20 cells from seven mice). *p < 0.05, ***p < 0.001, two-way ANOVA with Bonferroni post hoc test, data are represented as mean ± SEM.

(B) Traces of eIPSCs and quantification of eIPSC amplitudes recorded in GCs of mice treated with GCV (WT-TK$^-$, n = 12 cells from four mice; WT-TK$^+$, n = 7 cells from three mice; APP/PS1-TK$^-$, n = 6 cells from three mice; APP/PS1-TK$^+$, n = 11 cells from five mice). **p < 0.01, ***p < 0.001, two-way ANOVA with Bonferroni post hoc test, data are represented as mean ± SEM.

(C and D) Traces of mEPSCs (C) and mIPSC (D) recorded in GCs of WT-TK$^-$, WT-TK$^+$, APP/PS1-TK$^-$, and APP/PS-TK$^+$ mice treated with GCV.

(E and G) Cumulative fraction plots and quantification of mEPSC amplitudes (E) and frequency (G) in GCs of WT-TK$^-$ (n = 8 cells from four mice), WT-TK$^+$ (n = 10 cells from three mice), APP/PS1-TK$^-$ (n = 12 cells from six mice), and APP/PS1-TK$^+$ (n = 12 cells from four mice) mice treated with GCV. Two-way ANOVA for (E): genotype (APP), $F_{(1,38)}$ = 6.746, p = 0.0133; ablating aNSCs, $F_{(1,38)}$ = 7.817, p = 0.0081; interaction, $F_{(1,38)}$ = 2.543, p = 0.1197; *p < 0.05 with Bonferroni post hoc test. Data are represented as mean ± SEM.

(F and H) Cumulative fraction plots and quantification of mIPSC amplitudes (F) and frequency (H) in WT-TK$^-$ (n = 12 cells from four mice), WT-TK$^+$ (n = 10 cells from three mice), APP/PS1-TK$^-$ (n = 10 cells from three mice), and APP/PS1-TK$^+$ (n = 13 cells from five mice) mice treated with GCV. Two-way ANOVA for (F): genotype (APP), $F_{(1,41)}$ = 5.442, p = 0.0246; ablating aNSCs, $F_{(1,41)}$ = 3.708, p = 0.0611; interaction, $F_{(1,41)}$ = 3.918, p < 0.0545; *p < 0.05 with Bonferroni post hoc test. Data are represented as mean ± SEM.

cognition (Palop et al., 2007); (4) similar to our results in AD mice, reducing aberrant newborn neurons by ablation of aNSCs improves hippocampus-dependent memory in an epilepsy model (Cho et al., 2015). Therefore, both increasing healthy new neurons and reducing abnormal new neurons could be beneficial for cognitive functions in AD mice.

Different from our results, Hollands et al. (2017) reported that depletion of adult neurogenesis mildly exacerbated cognitive deficits in APPswe/PS1ΔE9 mice. However, they started the treatment at a very young age (right after weaning) with valganciclovir (v-GCV) (~90 mg/kg/day) for 2 months. On one hand, v-GCV treatment in AD mice expressing nestin-TK at a very young age may target not only adult neurogenesis but also other cells in the hippocampus, such as GCs and glia. On the other hand, while Snyder et al. (2011) showed that approximately 35 mg/kg/day of v-GCV is enough to inhibit adult neurogenesis, ~90 mg/kg/day of v-GCV for 2 months may induce side effects such as gastrointestinal inflammation (Bush et al., 1998). In another study, Choi et al. (2018) reported that ablating adult neurogenesis was associated with worsening cognition in 5-month-old 5×FAD mice. However, this effect could be observed only when the inhibition of adult neurogenesis was accompanied by loss of mature GCs and synaptic markers, and only inhibiting adult neurogenesis at very early age (6 weeks) (Choi et al., 2018). Therefore, in our opinion, although worsened behavioral functions were

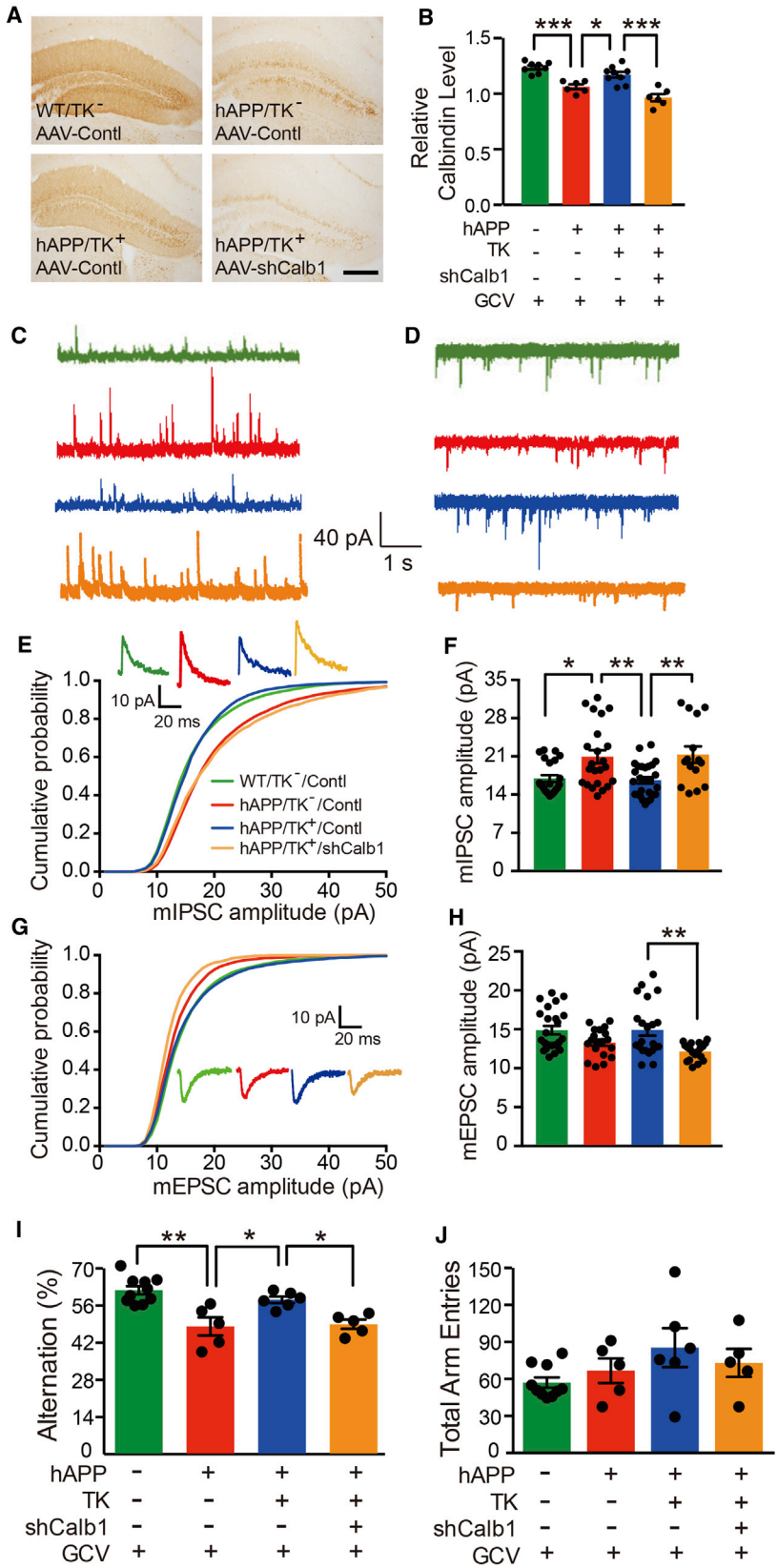

Figure 7. Hippocampal Knockdown of Calbindin Abolished the Effects of aNSC Ablation on Synaptic and Cognitive Functions in hAPP-J20 Mice

(A) Calbindin expression in the DG of the hippocampus. Scale bar, 500 μm.

(B) Quantification of the relative calbindin level in the DG of the hippocampus. Green, WT, n = 8; red, hAPP-J20, n = 6; blue, aNSC-deleted hAPP-J20, n = 9; brown, aNSC-deleted hAPP-J20 with injection of AAV-shCalb1, n = 6. All mice were treated with GCV. *p < 0.05, ***p < 0.001, one-way ANOVA with Tukey post hoc test, data are represented as mean ± SEM.

(C and D) Traces of mIPSCs (C) and mEPSCs (D) recorded in GCs of WT (green), hAPP-J20 (red), aNSC-deleted hAPP-J20 (blue), and aNSC-deleted hAPP-J20 with injection of AAV-shCalb1 (brown).

(E and F) Cumulative fraction plots (E) and quantification (F) of mIPSC amplitudes in GCs of WT (green, n = 23 cells from five mice), hAPP-J20 (red, n = 23 cells from five mice), aNSC-deleted hAPP-J20 (blue, n = 27 cells from five mice), and aNSC-deleted hAPP-J20 with injection of AAV-shCalb1 (brown, n = 15 cells from three mice) mice. All mice were treated with GCV. *p < 0.05, **p < 0.01, one-way ANOVA with Tukey post hoc test, data are represented as mean ± SEM.

(G and H) Cumulative fraction plots (G) and quantification (H) of mEPSC amplitudes in GCs of WT (green, n = 24 cells from five mice), hAPP-J20 (red, n = 19 cells from five mice), aNSC-deleted hAPP-J20 (blue, n = 22 cells from five mice), and aNSC-deleted hAPP-J20 with injection of AAV-shCalb1 (brown, n = 19 cells from three mice) mice. All mice were treated with GCV. **p < 0.01, one-way ANOVA with Tukey post hoc test, data are represented as mean ± SEM.

(I and J) Y-maze tests showing percentage of alterations (I) and total arm entries (J) in WT (green, n = 10), hAPP-J20 (red, n = 5), aNSC-deleted hAPP-J20 (blue, n = 6), and aNSC-deleted hAPP-J20 with injection of AAV-shCalb1 (brown, n = 5) mice. All mice were treated with GCV. *p < 0.05, **p < 0.01, one-way ANOVA with Tukey post hoc test, data are represented as mean ± SEM.

See also Figure S7.

observed in AD mice, data from these studies did not provide conclusive evidence that these behavioral changes were caused by ablating adult neurogenesis.

Adult-born new neurons are abnormal in the hippocampus of AD mice (Krezymon et al., 2013; Richetin et al., 2015; Sun et al., 2009). However, not all new neurons are abnormal. The current approaches to ablate aNSCs in our study and other studies (Choi et al., 2018; Hollands et al., 2017) could not distinguish normal from abnormal new neurons in AD mice. Better approaches to target specific populations of new neurons will facilitate the complete understanding of the effects of modulating adult neurogenesis on AD. Similarly, it will be ideal to specifically increase the number of healthy new neurons but not simply increase the number of new neurons in the hippocampus of AD mice.

In summary, we demonstrated that ablating aNSCs improved cognitive functions in AD mice. This effect was associated with the restoration of synaptic transmission in GCs, and the altered expression of calbindin was an important mediator during this process. We also believe that the effects of deleting abnormal new neurons and enhancing healthy neurogenesis on AD are not mutually exclusive. In future studies, developing better strategies to target specific populations of new neurons (either decreasing or increasing) will help us to fully appreciate the effects of modulating adult neurogenesis on cognitive functions in AD. It is also important to further dissect the effects of modulating adult neurogenesis on the activity of neural circuits in the hippocampus of AD mice.

EXPERIMENTAL PROCEDURES

Animals

APP/PS1 (Jax, 34,832) and hAPP-J20 mice (Jax MMRRC, 034836) were used as AD models. GFAP-TK mice (Snyder et al., 2011) were provided by Dr. Tianming Gao (Southern Medical University, China) with permission from Dr. Heather Cameron (NIH). POMC-GFP mice (Jax, 009593) were used to visualize newborn neurons in the hippocampus. All mice were housed under standard conditions at 22°C and a 12 h light:dark cycle with free access to food and water. All experiments were approved by the Institutional Animal Care and Use Committee of the Zhejiang University.

Drug Treatments

GCV treatment: TK^- and TK^+ mice of WT, APP/PS1, and hAPP-J20 were treated with GCV (Roche; in 0.9% sterile saline) at 20 mg/kg/day via subcutaneous osmotic mini-pumps (Model, 2004; Alzet; 0.25 μL/h release rate).

MAM treatment: hAPP-J20 mice received an intraperitoneal injection of MAM (7 mg/kg; Wako pure chemical industries, no. 136–16303) or vehicle (saline) once per day for seven consecutive days before electrophysiological recordings and behavioral tests. MAM treatment started from approximately the age of 4.5–5 months.

Stereotaxic Injection of Virus

AAV-shCalb1 (pAKD-CMV-bGlobin-eGFP-H1-Calb1, 3.89×10^{12} viral genomes/mL) (Li et al., 2017) was stereotaxically injected into the DG (0.4 μL/hemisphere at a perfusion rate of 0.1 μL/min; anterior-posterior, −2.1 mm; lateral, ±1.7 mm; and vertical, −2.0 mm; the bregma was used as the reference point) to knock down the expression of calbindin in the hippocampus of hAPP-J20 mice after ablation of aNSCs.

To label newborn neurons, a retroviral vector expressing eGFP (Zhao et al., 2006) was injected into the hippocampus of WT-TK^- and APP/PS1-TK^- mice or WT/veh and hAPP-J20/veh mice (around 4 months old) using the same coordinates as above. Dendritic length and spine density of newborn neurons were analyzed 28 days after the injection of virus as described previously (Sun et al., 2009).

ELISA

ELISA for quantification of Aβ was performed as described previously (JohnsonWood et al., 1997). Detailed information for ELISA is provided in the Supplemental Experimental Procedures.

Immunostaining and Quantification

Immunofluorescence and immunohistochemistry were performed as described previously (Zhang et al., 2017). Details of staining and quantification are provided in Supplemental Experimental Procedures.

Western Blotting Analysis

Western blotting was performed as described previously (Zhang et al., 2017) to examine the expression of hAPP, fragments of hAPP, and PS1. Details are provided in the Supplemental Experimental Procedures.

Behavioral Tests

For behavioral analyses (MWM and Y-maze tests), mouse genotypes were blinded. Ages of mice are indicated in the results and figure legends. MWM and Y maze were performed as described previously (Zhang et al., 2017). Details are provided in the Supplemental Experimental Procedures.

Electrophysiology

Whole-cell recordings were performed to examine the mini-, spontaneous and evoked inhibitory postsynaptic currents and excitatory postsynaptic currents in GCs. Detailed information is provided in the Supplemental Experimental Procedures.

Statistical Analyses

Statistical analyses were performed with Graphpad Prism 5 (San Diego, CA). All data were presented as mean ± SEM. Differences among multiple means were evaluated by one-way ANOVA with Tukey post tests, two-way ANOVA with Bonferroni post tests, or three-way ANOVA. Differences between two means were assessed

with paired or unpaired, two-tailed t test. Only values with $p < 0.05$ were accepted as significant.

DATA AND CODE AVAILABILITY

The data that support the findings of this study are available from the corresponding author upon reasonable request.

SUPPLEMENTAL INFORMATION

Supplemental Information can be found online at https://doi.org/10.1016/j.stemcr.2020.12.003.

AUTHORS CONTRIBUTIONS

B.S., X.Z., and Y.M. conceived and designed the study. X.Z., F.M., Y.H., D.W., E.Y., X.W., M.Z., J.W., and G.P. performed the experiments. X.Z., Y.M., Y.H., H.S., Q.S., X.L., B.L., Y.Z., and B.S. analyzed the data. B.S. and X.Z. wrote the manuscript with inputs from other authors. B.S. supervised the project.

CONFLICTS OF INTEREST

The authors declare no competing interests.

ACKNOWLEDGMENTS

We thank Drs Heather Cameron and Tianming Gao for the GFAP-TK mice; Dr. Edward Koo for CT-15 antibody; Dr. Fred Gage for retroviral vector expressing eGFP; and Janssen Research & Development, L.L.C., for antibodies 266, 21F12, and 3D6. Dr. Xiaodong Wang provided suggestions for behavioral tests and design of AAV-shCalb1.We also thank the Core Facilities of Zhejiang University School of Medicine for technical support. This work was supported by grants from National Key Research and Development Program of China (2019YFA0110103), Natural Science Foundation of Zhejiang Province (LZ19C090001), National Natural Science Foundation of China (31871025, 32071031, 91132713), National Key R&D Program of China (2017YFE0196600), National Basic Research Program of China (973 Program) (2014CB964602 and 2013CB530902), Zhejiang Provincial Natural Science Foundation (LQ20C090002), the Science and Technology Planning Project of Zhejiang Province (2017C03011), and Chinese Ministry of Education Project 111 (B13026).

Received: June 9, 2020
Revised: November 30, 2020
Accepted: December 1, 2020
Published: December 30, 2020

REFERENCES

Akers, K.G., Martinez-Canabal, A., Restivo, L., Yiu, A.P., De Cristofaro, A., Hsiang, H.L., Wheeler, A.L., Guskjolen, A., Niibori, Y., Shoji, H., et al. (2014). Hippocampal neurogenesis regulates forgetting during adulthood and infancy. Science *344*, 598–602.

Anacker, C., and Hen, R. (2017). Adult hippocampal neurogenesis and cognitive flexibility - linking memory and mood. Nat. Rev. Neurosci. *18*, 335–346.

Anacker, C., Luna, V.M., Stevens, G.S., Millette, A., Shores, R., Jimenez, J.C., Chen, B., and Hen, R. (2018). Hippocampal neurogenesis confers stress resilience by inhibiting the ventral dentate gyrus. Nature *559*, 98–102.

Boldrini, M., Fulmore, C.A., Tartt, A.N., Simeon, L.R., Pavlova, I., Poposka, V., Rosoklija, G.B., Stankov, A., Arango, V., Dwork, A.J., et al. (2018). Human hippocampal neurogenesis persists throughout aging. Cell Stem Cell *22*, 589–599.

Bond, A.M., Ming, G.L., and Song, H.J. (2015). Adult mammalian neural stem cells and neurogenesis: five decades later. Cell Stem Cell *17*, 385–395.

Bush, T.G., Savidge, T.C., Freeman, T.C., Cox, H.J., Campbell, E.A., Mucke, L., Johnson, M.H., and Sofroniew, M.V. (1998). Fulminant jejuno-ileitis following ablation of enteric glia in adult transgenic mice. Cell *93*, 189–201.

Cho, K.O., Lybrand, Z.R., Ito, N., Brulet, R., Tafacory, F., Zhang, L., Good, L., Ure, K., Kernie, S.G., Birnbaum, S.G., et al. (2015). Aberrant hippocampal neurogenesis contributes to epilepsy and associated cognitive decline. Nat. Commun. *6*, 6606.

Choi, S.H., Bylykbashi, E., Chatila, Z.K., Lee, S.W., Pulli, B., Clemenson, G.D., Kim, E., Rompala, A., Oram, M.K., Asselin, C., et al. (2018). Combined adult neurogenesis and BDNF mimic exercise effects on cognition in an Alzheimer's mouse model. Science *361*, eaan8821.

Clelland, C.D., Choi, M., Romberg, C., Clemenson, G.D., Fragniere, A., Tyers, P., Jessberger, S., Saksida, L.M., Barker, R.A., Gage, F.H., et al. (2009). A functional role for adult hippocampal neurogenesis in spatial pattern separation. Science *325*, 210–213.

Comings, D.E., and MacMurray, J.P. (2000). Molecular heterosis: a review. Mol. Genet. Metab. *71*, 19–31.

Ding, Z., Mathur, V., Ho, P.P., James, M.L., Lucin, K.M., Hoehne, A., Alabsi, H., Gambhir, S.S., Steinman, L., Luo, J., et al. (2014). Antiviral drug ganciclovir is a potent inhibitor of microglial proliferation and neuroinflammation. J. Exp. Med. *211*, 189–198.

Drew, L.J., Kheirbek, M.A., Luna, V.M., Denny, C.A., Cloidt, M.A., Wu, M.V., Jain, S., Scharfman, H.E., and Hen, R. (2016). Activation of local inhibitory circuits in the dentate gyrus by adult-born neurons. Hippocampus *26*, 763–778.

Eriksson, P.S., Perfilieva, E., Bjork-Eriksson, T., Alborn, A.M., Nordborg, C., Peterson, D.A., and Gage, F.H. (1998). Neurogenesis in the adult human hippocampus. Nat. Med. *4*, 1313–1317.

Fiorentini, A., Rosi, M.C., Grossi, C., Luccarini, I., and Casamenti, F. (2010). Lithium improves hippocampal neurogenesis, neuropathology and cognitive functions in APP mutant mice. PLoS One *5*, e12382.

Ge, S.Y., Yang, C.H., Hsu, K.S., Ming, G.L., and Song, H.J. (2007). A critical period for enhanced synaptic plasticity in newly generated neurons of the adult brain. Neuron *54*, 559–566.

Gu, Y., Arruda-Carvalho, M., Wang, J., Janoschka, S.R., Josselyn, S.A., Frankland, P.W., and Ge, S.Y. (2012). Optical controlling reveals time-dependent roles for adult-born dentate granule cells. Nat. Neurosci. *15*, 1700–1706.

Hollands, C., Tobin, M.K., Hsu, M., Musaraca, K., Yu, T.S., Mishra, R., Kernie, S.G., and Lazarov, O. (2017). Depletion of adult neurogenesis exacerbates cognitive deficits in Alzheimer's disease

by compromising hippocampal inhibition. Mol. Neurodegener. *12*, 64.

Jackson, H.M., Soto, I., Graham, L.C., Carter, G.W., and Howell, G.R. (2013). Clustering of transcriptional profiles identifies changes to insulin signaling as an early event in a mouse model of Alzheimer's disease. BMC Genomics *14*, 831.

Jankowsky, J.L., Fadale, D.J., Anderson, J., Xu, G.M., Gonzales, V., Jenkins, N.A., Copeland, N.G., Lee, M.K., Younkin, L.H., Wagner, S.L., et al. (2004). Mutant presenilins specifically elevate the levels of the 42 residue beta-amyloid peptide in vivo: evidence for augmentation of a 42-specific gamma secretase. Hum. Mol. Genet. *13*, 159–170.

Jin, K.L., Galvan, V., Xie, L., Mao, X.O., Gorostiza, O.F., Bredesen, D.E., and Greenberg, D.A. (2004). Enhanced neurogenesis in Alzheimer's disease transgenic (PDGF-APP(sw,lnd))mice. Proc. Natl. Acad. Sci. U S A *101*, 13363–13367.

JohnsonWood, K., Lee, M., Motter, R., Hu, K., Gordon, G., Barbour, R., Khan, K., Gordon, M., Tan, H., Games, D., et al. (1997). Amyloid precursor protein processing and A beta(42) deposition in a transgenic mouse model of Alzheimer disease. Proc. Natl. Acad. Sci. U S A *94*, 1550–1555.

Kempermann, G., Gage, F.H., Aigner, L., Song, H.J., Curtis, M.A., Thuret, S., Kuhn, H.G., Jessberger, S., Frankland, P.W., Cameron, H.A., et al. (2018). Human adult neurogenesis: evidence and remaining questions. Cell Stem Cell *23*, 25–30.

Krezymon, A., Richetin, K., Halley, H., Roybon, L., Lassalle, J.M., Frances, B., Verret, L., and Rampon, C. (2013). Modifications of hippocampal circuits and early disruption of adult neurogenesis in the Tg2576 mouse model of Alzheimer's disease. PLoS One *8*, e76497.

Kuhn, H.G., Toda, T., and Gage, F.H. (2018). Adult hippocampal neurogenesis: a coming-of-age story. J. Neurosci. *38*, 10401–10410.

Li, J.T., Xie, X.M., Yu, J.Y., Sun, Y.X., Liao, X.M., Wang, X.X., Su, Y.A., Liu, Y.J., Schmidt, M.V., Wang, X.D., et al. (2017). Suppressed calbindin levels in hippocampal excitatory neurons mediate stress-induced memory loss. Cell Rep. *21*, 891–900.

Lucassen, P.J., Fitzsimons, C.P., Salta, E., and Maletic-Savatic, M. (2020). Adult neurogenesis, human after all (again): classic, optimized, and future approaches. Behav. Brain Res. *381*, 112458.

Mathur, V., Burai, R., Vest, R.T., Bonanno, L.N., Lehallier, B., Zardeneta, M.E., Mistry, K.N., Do, D., Marsh, S.E., Abud, E.M., et al. (2017). Activation of the STING-dependent type I interferon response reduces microglial reactivity and neuroinflammation. Neuron *96*, 1290–1302.e6.

Minkeviciene, R., Ihalainen, J., Malm, T., Matilainen, O., Keksa-Goldsteine, V., Goldsteins, G., Iivonen, H., Leguit, N., Glennon, J., Koistinaho, J., et al. (2008). Age-related decrease in stimulated glutamate release and vesicular glutamate transporters in APP/PS1 transgenic and wild-type mice. J. Neurochem. *105*, 584–594.

Molinari, S., Battini, R., Ferrari, S., Pozzi, L., Killcross, A.S., Robbins, T.W., Jouvenceau, A., Billard, J.M., Dutar, P., Lamour, Y., et al. (1996). Deficits in memory and hippocampal long-term potentiation in mice with reduced calbindin D-28K expression. Proc. Natl. Acad. Sci. U S A *93*, 8028–8033.

Moreno-Jimenez, E.P., Flor-Garcia, M., Terreros-Roncal, J., Rabano, A., Cafini, F., Pallas-Bazarra, N., Avila, J., and Llorens-Martin, M. (2019). Adult hippocampal neurogenesis is abundant in neurologically healthy subjects and drops sharply in patients with Alzheimer's disease. Nat. Med. *25*, 554–560.

Mucke, L., Masliah, E., Yu, G.Q., Mallory, M., Rockenstein, E.M., Tatsuno, G., Hu, K., Kholodenko, D., Johnson-Wood, K., and McConlogue, L. (2000). High-level neuronal expression of abeta 1-42 in wild-type human amyloid protein precursor transgenic mice: synaptotoxicity without plaque formation. J. Neurosci. *20*, 4050–4058.

Musiek, E.S., and Holtzman, D.M. (2015). Three dimensions of the amyloid hypothesis: time, space and 'wingmen. Nat. Neurosci. *18*, 800–806.

Overstreet, L.S., Hentges, S.T., Bumaschny, V.F., de Souza, F.S.J., Smart, J.L., Santangelo, A.M., Low, M.J., Westbrook, G.L., and Rubinstein, M. (2004). A transgenic marker for newly born granule cells in dentate gyrus. J. Neurosci. *24*, 3251–3259.

Palop, J.J., Chin, J., Roberson, E.D., Wang, J., Thwin, M.T., Bien-Ly, N., Yoo, J., Ho, K.O., Yu, G.Q., Kreitzer, A., et al. (2007). Aberrant excitatory neuronal activity and compensatory remodeling of inhibitory hippocampal circuits in mouse models of Alzheimer's disease. Neuron *55*, 697–711.

Palop, J.J., Jones, B., Kekonius, L., Chin, J., Yu, G.Q., Raber, J., Masliah, E., and Mucke, L. (2003). Neuronal depletion of calcium-dependent proteins in the dentate gyrus is tightly linked to Alzheimer's disease-related cognitive deficits. Proc. Natl. Acad. Sci. U S A *100*, 9572–9577.

Pan, H.Y., Wang, D.P., Zhang, X.Q., Zhou, D.M., Zhang, H., Qian, Q., He, X., Liu, Z.L., Liu, Y.J., Zheng, T.T., et al. (2016). Amyloid beta is not the major factor accounting for impaired adult hippocampal neurogenesis in mice overexpressing amyloid precursor protein. Stem Cell Rep. *7*, 707–718.

Richetin, K., Leclerc, C., Toni, N., Gallopin, T., Pech, S., Roybon, L., and Rampon, C. (2015). Genetic manipulation of adult-born hippocampal neurons rescues memory in a mouse model of Alzheimer's disease. Brain *138*, 440–455.

Sanchez, P.E., Zhu, L., Verret, L., Vossel, K.A., Orr, A.G., Cirrito, J.R., Devidze, N., Ho, K., Yu, G.Q., Palop, J.J., et al. (2012). Levetiracetam suppresses neuronal network dysfunction and reverses synaptic and cognitive deficits in an Alzheimer's disease model. Proc. Natl. Acad. Sci. U S A *109*, E2895–E2903.

Scharfman, H., Goodman, J., Macleod, A., Phani, S., Antonelli, C., and Croll, S. (2005). Increased neurogenesis and the ectopic granule cells after intrahippocampal BDNF infusion in adult rats. Exp. Neurol. *192*, 348–356.

Schmidt-Hieber, C., Jonas, P., and Bischofberger, J. (2004). Enhanced synaptic plasticity in newly generated granule cells of the adult hippocampus. Nature *429*, 184–187.

Selkoe, D.J., and Hardy, J. (2016). The amyloid hypothesis of Alzheimer's disease at 25years. EMBO Mol. Med. *8*, 595–608.

Shors, T.J., Miesegaes, G., Beylin, A., Zhao, M.R., Rydel, T., and Gould, E. (2001). Neurogenesis in the adult is involved in the formation of trace memories. Nature *410*, 372–376.

Snyder, J.S., Soumier, A., Brewer, M., Pickel, J., and Cameron, H.A. (2011). Adult hippocampal neurogenesis buffers stress responses and depressive behaviour. Nature *476*, 458–461.

Spalding, K.L., Bergmann, O., Alkass, K., Bernard, S., Salehpour, M., Huttner, H.B., Bostrom, E., Westerlund, I., Vial, C., Buchholz, B.A., et al. (2013). Dynamics of hippocampal neurogenesis in adult humans. Cell *153*, 1219–1227.

Sun, B.G., Halabisky, B., Zhou, Y.G., Palop, J.J., Yu, G.Q., Mucke, L., and Gan, L. (2009). Imbalance between GABAergic and glutamatergic transmission impairs adult neurogenesis in an animal model of Alzheimer's disease. Cell Stem Cell *5*, 624–633.

Sun, B.G., Zhou, Y.G., Halabisky, B., Lo, I., Cho, S.H., Mueller-Steiner, S., Devidze, N., Wang, X., Grubb, A., and Gan, L. (2008). Cystatin C-cathepsin B axis regulates amyloid beta levels and associated neuronal deficits in an animal model of Alzheimer's disease. Neuron *60*, 247–257.

Tobin, M.K., Musaraca, K., Disouky, A., Shetti, A., Bheri, A., Honer, W.G., Kim, N., Dawe, R.J., Bennett, D.A., Arfanakis, K., et al. (2019). Human hippocampal neurogenesis persists in aged adults and Alzheimer's disease patients. Cell Stem Cell *24*, 974–982.e3.

Toda, T., Parylak, S.L., Linker, S.B., and Gage, F.H. (2019). The role of adult hippocampal neurogenesis in brain health and disease. Mol. Psychiatry *24*, 67–87.

Unger, M.S., Marschallinger, J., Kaindl, J., Hofling, C., Rossner, S., Heneka, M.T., Van der Linden, A., and Aigner, L. (2016). Early changes in hippocampal neurogenesis in transgenic mouse models for Alzheimer's disease. Mol. Neurobiol. *53*, 5796–5806.

van Praag, H., Kempermann, G., and Gage, F.H. (1999). Running increases cell proliferation and neurogenesis in the adult mouse dentate gyrus. Nat. Neurosci. *2*, 266–270.

van Praag, H., Schinder, A.F., Christie, B.R., Toni, N., Palmer, T.D., and Gage, F.H. (2002). Functional neurogenesis in the adult hippocampus. Nature *415*, 1030–1034.

Vivar, C., Potter, M.C., Choi, J., Lee, J.Y., Stringer, T.P., Callaway, E.M., Gage, F.H., Suh, H., and van Praag, H. (2012). Monosynaptic inputs to new neurons in the dentate gyrus. Nat. Commun. *3*, 1107.

Wang, J.M., Singh, C., Liu, L.F., Irwin, R.W., Chen, S.H., Chung, E.J., Thompson, R.F., and Brinton, R.D. (2010). Allopregnanolone reverses neurogenic and cognitive deficits in mouse model of Alzheimer's disease. Proc. Natl. Acad. Sci. U S A *107*, 6498–6503.

Wright, A.L., Zinn, R., Hohensinn, B., Konen, L.M., Beynon, S.B., Tan, R.P., Clark, I.A., Abdipranoto, A., and Vissel, B. (2013). Neuroinflammation and neuronal loss precede ab plaque deposition in the hAPP-J20 mouse model of Alzheimer's disease. PLoS One *8*, e59586.

You, J.C., Muralidharan, K., Park, J.W., Petrof, I., Pyfer, M.S., Corbett, B.F., LaFrancois, J.J., Zheng, Y., Zhang, X.H., Mohila, C.A., et al. (2017). Epigenetic suppression of hippocampal calbindin-D28k by Delta FosB drives seizure-related cognitive deficits. Nat. Med. *23*, 1377–1383.

Zhang, H., Zhang, L., Zhou, D.M., He, X., Wang, D.P., Pan, H.Y., Zhang, X.Q., Mei, Y.F., Qian, Q., Zheng, T.T., et al. (2017). Ablating ErbB4 in PV neurons attenuates synaptic and cognitive deficits in an animal model of Alzheimer's disease. Neurobiol. Dis. *106*, 171–180.

Zhao, C.M., Teng, E.M., Summers, R.G., Ming, G.L., and Gage, F.H. (2006). Distinct morphological stages of dentate granule neuron maturation in the adult mouse hippocampus. J. Neurosci. *26*, 3–11.